Calculation of neutron-³He scattering up to 30 MeV

A. Deltuva

Institute of Theoretical Physics and Astronomy, Vilnius University, A. Goštauto 12, LT-01108 Vilnius, Lithuania

A. C. Fonseca

Centro de Física Nuclear da Universidade de Lisboa, P-1649-003 Lisboa, Portugal

Background: Microscopic calculations of four-body collisions become very challenging in the energy regime above the threshold for four free particles. The neutron-³He scattering is an example of such processes with elastic, rearrangement, and breakup channels.

Purpose: We aim to calculate observables for elastic and inelastic neutron-³He reactions up to 30 MeV neutron energy using realistic nuclear force models.

Methods: We solve the Alt, Grassberger, and Sandhas (AGS) equations for the four-nucleon transition operators in the momentum-space framework. The complex-energy method with special integration weights is applied to deal with the complicated singularities in the kernel of AGS equations.

Results: We obtain fully converged results for the differential cross section and neutron analyzing power in the neutron-³He elastic scattering as well as the total cross sections for inelastic reactions. Several realistic potentials are used, including one with an explicit Δ isobar excitation.

Conclusions: There is reasonable agreement between the theoretical predictions and experimental data for the neutron-³He scattering in the considered energy regime. The most remarkable disagreements are seen around the minimum of the differential cross section and the extrema of the neutron analyzing power. The breakup cross section increases with energy exceeding rearrangement channels above 23 MeV.

I. INTRODUCTION

Experimentally, four-nucleon ($4N$) physics is studied most extensively through proton-³He (p-³He) and deuteron-deuteron (d-d) reactions [1], i.e., charged particle beams and nonradioactive targets. The $p + $³He system is simpler since it involves three protons and one neutron and, furthermore, only elastic and breakup channels exist. Theoretically, below breakup threshold $p + $³He scattering constitutes a single-channel problem, making it also simpler to calculate. Indeed, accurate numerical calculations for low-energy p-³He elastic scattering have been performed using several rigorous approaches, i.e., the hyperspherical harmonics (HH) expansion method [2,3], the Faddeev-Yakubovsky (FY) equations [4] for the wave function components [5], and the Alt, Grassberger and Sandhas (AGS) equations [6] for transition operators [7,8]. The latter method uses the momentum-space framework, while the former two are implemented in the coordinate space framework. All these methods were benchmarked in Ref. [9] below breakup threshold for observables in neutron-³H (n-³H) and p-³He elastic scattering; good agreement between calculations was found, confirming their reliability.

However, the physics of reactions in coupled proton-³H (p-³H), neutron-³He (n-³He) and d-d systems is more rich. The scattering process in these systems resembles a typical nuclear reaction where, depending on the available energy, elastic, charge exchange, transfer, and breakup reactions may take place simultaneously. At the same time such reactions are more difficult to calculate. Indeed, the coordinate space methods are limited so far to processes up to n-³He threshold [10,11]. In contrast, the momentum-space calculations are available for

all elastic and rearrangement p-³H, n-³He, and d-d reactions below three-cluster breakup threshold [12,13]. However, the extension to higher energies constitutes a major difficulty, since the asymptotic boundary conditions in coordinate space become highly nontrivial due to open two-, three-, and four-cluster channels. In the momentum-space framework this is reflected in a very complicated structure of singularities in the kernel of the integral equations. Formally, these difficulties can be avoided by rotation to complex coordinates [14,15] or continuation to complex energy [16,17] that lead to bound-state-like boundary conditions and nonsingular kernels. However, further technical complications arise in practical calculations, especially when using realistic nuclear force models. Although the solution of FY equations for n-³H scattering with modern potentials using complex scaling is under way [18], at present the only realistic calculations of $4N$ scattering above $4N$ threshold are performed using the momentum-space AGS equations [19,20], but limited to n-³H and p-³He elastic scattering. The complex energy method [17,21] was used to deal with the complicated singularities in the four-particle scattering equations; its accuracy and practical applicability were greatly improved by a special integration method [19].

In the present work, following the ideas of Refs. [19,20], we calculate $n + $³He elastic and inelastic scattering over a wide range of neutron beam energies up to $E_n = 30$ MeV. The pp Coulomb interaction is included using the method of screening and renormalization [22,23]; see Refs. [8,24] for more details on the practical implementation. Within this method the standard AGS scattering equations for short-range potentials are applicable. Compared to our previous

p-^{3}He scattering calculations above breakup threshold [20], an additional complication for $n + {}^3$He reactions is the presence of the rearrangement channels and the mixing of total isospin $\mathcal{T} = 0$ and 1 states. On the other hand, $n + {}^3$He calculations are somehow simpler than those for $p + {}^3$H or $d + d$, since there is no long-range Coulomb interaction in the asymptotic $n + {}^3$He state, making the convergence of the partial-wave expansion slightly faster.

In Sec. II we describe the theoretical formalism and in Sec. III we present the numerical results. The summary is given in Sec. IV.

II. 4N SCATTERING EQUATIONS

We treat protons and neutron as identical particles in the isospin formalism and therefore use the symmetrized version of the AGS equations [7] that are integral equations for the four-particle transition operators $\mathcal{U}_{\beta\alpha}$, i.e.,

$$\mathcal{U}_{11} = -(G_0 t G_0)^{-1} P_{34} - P_{34} U_1 G_0 t G_0 \mathcal{U}_{11} + U_2 G_0 t G_0 \mathcal{U}_{21}, \quad (1a)$$

$$\mathcal{U}_{21} = (G_0 t G_0)^{-1}(1 - P_{34}) + (1 - P_{34}) U_1 G_0 t G_0 \mathcal{U}_{11}. \quad (1b)$$

For $n + {}^3$He scattering the initial two-cluster partition that is of $3 + 1$ type is labeled as $\alpha = 1$, whereas $\beta = 2$ corresponds to the $2 + 2$ partition. They are chosen as (12,3)4 and (12)(34), respectively; in the system of four identical particles there are no other distinct two-cluster partitions. The transition operators U_α for these $3 + 1$ and $2 + 2$ subsystems are obtained from the respective integral equations

$$U_\alpha = P_\alpha G_0^{-1} + P_\alpha t G_0 U_\alpha. \quad (2)$$

The pair (12) transition matrix $t = v + vG_0 t$ is derived from the corresponding two-nucleon potential v that, besides the nuclear part, includes also the screened Coulomb potential w_R for the pp pair. The screening function is taken over from Refs. [8,12] but the dependence on the screening radius R is suppressed in our notation. The permutation operators P_{ab} of particles a and b and their combinations $P_1 = P_{12} P_{23} + P_{13} P_{23}$ and $P_2 = P_{13} P_{24}$ together with a special choice of the basis states ensure the full antisymmetry of the four-nucleon system. The basis states must be antisymmetric under exchange of two particles in the subsystem (12) for the $3 + 1$ partition and in (12) and (34) for the $2 + 2$ partition. All transition operators acquire their dependence on the available energy E through the free resolvent

$$G_0 = (E + i\varepsilon - H_0)^{-1}, \quad (3)$$

with the complex energy $E + i\varepsilon$ and the free Hamiltonian H_0.

Although the physical scattering process corresponds to the $\varepsilon \to +0$ limit, the AGS equations are solved numerically at a complex energy $E + i\varepsilon$ with finite positive ε. This way we avoid the very complicated singularity structure of the kernel and are faced with quasisingularities, that can be accurately integrated over using a special integration method developed in Ref. [19]. The singularities (quasisingularities for finite ε) of

the AGS equations correspond to open channels. In addition to elastic and three- and four-cluster breakup channels, present in the n-^{3}H and p-^{3}He scattering [19,20], in the $n + {}^3$He reaction there are the rearrangement channels $p + {}^3$H and $d + d$. They are treated in the same way as the elastic $n + {}^3$He channel. The limit $\varepsilon \to +0$ needed for the calculation of scattering amplitudes and observables is obtained by the extrapolation of finite ε results. Previous calculations [19,21] employed the point method [25]. In the present work, as an additional accuracy check, we use also the cubic spline extrapolation with a nonstandard choice of boundary conditions, namely, the one ensuring continuity of the third derivative [26]. These two different methods lead to indistinguishable results confirming the reliability of the extrapolation procedure. We use ε ranging from 1 to 2 MeV at the lowest considered energies and from 2 to 4 MeV at the highest energies. About 30 grid points for the discretization of each momentum variable are used.

As mentioned, the potential v for the pp pair must include both the nuclear and the screened Coulomb potential w_R; see Refs. [8,12] for more details. The limit $\varepsilon \to +0$ is calculated separately for each value of the Coulomb screening radius R and the renormalization procedure [8,12] is performed subsequently. Thus, the scattering amplitude connecting the initial $n + {}^3$He state with any two-cluster state is given by

$$\langle \mathbf{p}_f | T_{fi} | \mathbf{p}_i \rangle = S_{\beta_f \alpha_i} \lim_{R \to \infty} \left[(Z_R^f)^{-\frac{1}{2}} \lim_{\varepsilon \to +0} \langle \phi_f | \mathcal{U}_{\beta_f \alpha_i} | \phi_i \rangle \right]. \quad (4)$$

Here, $|\phi_j\rangle = G_0 t P_{\alpha_j} |\phi_j\rangle$ are the Faddeev amplitudes of the initial (i) or final (f) channel states $|\Phi_j\rangle = (1 + P_{\alpha_j})|\phi_j\rangle$, whereas $S_{11} = 3$ and $S_{21} = \sqrt{3}$ are the weight factors resulting from the symmetrization. Note that the $d + d$ channel state requires explicit symmetrization under the exchange of two deuterons, since the employed basis states do not obey this symmetry. The initial and final bound state energies ϵ_j, relative two-cluster momenta $\mathbf{p}_j$ and reduced masses μ_j obey the on-shell relation $E = \epsilon_j + p_j^2/2\mu_j$. The renormalization factor Z_R^f is defined as in Refs. [8,12]; it is simply 1 for the $n + {}^3$He state which is not distorted by the long-range Coulomb interaction. In the present calculations we use $R = 16$ fm which is fully sufficient for convergence.

The spin-averaged differential cross section for the transition to the $n + {}^3$He, $p + {}^3$H or $d + d$ final state is

$$\frac{d\sigma}{d\Omega} = (2\pi)^4 \mu_i \mu_f \frac{p_f}{p_i} \frac{1}{N_{s_f}} \sum_{m_{s_i}, m_{s_f}} |\langle \mathbf{p}_f | T_{fi} | \mathbf{p}_i \rangle|^2, \quad (5)$$

where the summation runs over the initial and final spin projections m_{s_i} and m_{s_f}, and $N_{s_f} = 4$ is the number of initial spin states for two spin $\frac{1}{2}$ particles. The total cross section for a given reaction is obtained by integrating Eq. (5) over the solid angle 4π for $n + {}^3$He and $p + {}^3$H final states and 2π for $d + d$ final state.

The breakup amplitudes can be obtained from the half-shell matrix elements of $\mathcal{U}_{\beta\alpha}$ as described in Refs. [27,28]. However, in the present work we only calculate the total three- and four-cluster breakup cross section as the difference between

the total and all two-cluster cross sections. The total $n + {}^3$He cross section is obtained using the optical theorem as

$$\sigma_t = -16\pi^3 \frac{\mu_i}{p_i} \frac{1}{N_{s_f}} \sum_{m_{s_i}} \text{Im}\langle \mathbf{p}_i | T_{ii} | \mathbf{p}_i \rangle. \tag{6}$$

The AGS equations are solved by us in the momentum-space partial-wave framework. We define the states of the total angular momentum $\mathcal{J}$ with projection $\mathcal{M}$ as $|k_x k_y k_z [l_z(\{l_y[(l_x S_x)j_x s_y]S_y\}J_y s_z)S_z]\mathcal{JM}\rangle$ for the $3 + 1$ configuration and $|k_x k_y k_z (l_z\{l_x(l_x S_x)j_x [l_y(s_y s_z)S_y]j_y\}S_z)\mathcal{JM}\rangle$ for the $2 + 2$. In the literature they are called sometimes K-type and H-type basis states, respectively. Here $k_x, k_y,$ and k_z are the four-particle Jacobi momenta in the convention of Ref. [27], $l_x, l_y,$ and l_z are the associated orbital angular momenta, j_x and j_y are the total angular momenta of pairs (12) and (34), J_y is the total angular momentum of the (123) subsystem, s_y and s_z are the spins of nucleons 3 and 4, and S_x, S_y, and S_z are channel spins of two-, three-, and four-particle systems.

With respect to isospin, there are important differences as compared to previous n-^{3}H and p-^{3}He calculations. Two types of isospin states are used in the present calculations for the $3 + 1$ configuration: $|(T_x t_y)T_y M_y t_z m_z\rangle$ and $|[(T_x t_y)T_y t_z]\mathcal{T}\mathcal{M}_\mathcal{T}\rangle$. They are related by a simple unitary transformation with Clebsch-Gordan coefficients $\langle T_y M_y t_z m_z | \mathcal{T}\mathcal{M}_\mathcal{T}\rangle$. Here T_x is the isospin of the pair (12), $t_y = t_z = \frac{1}{2}$ are the isospins of nucleons 3 and 4, T_y is the isospin of the (123) subsystem, and $\mathcal{T}$ is the total isospin of the 4N system, with m_z, M_y, and $\mathcal{M}_\mathcal{T} = 0$ being the respective projections. For the $2 + 2$ configuration the isospin states are $|[T_x(t_y t_z)T_z]\mathcal{T}\mathcal{M}_\mathcal{T}\rangle$, with T_z being the isospin of the pair (34).

The eigenstates of the total isospin are more convenient to calculate the action of the permutation operator P_{34} and transformations between the K- and H-type states, since these operations conserve $\mathcal{T}$. In contrast, the $3 + 1$ channel states mix the total isospin but have fixed values of M_y and m_z, i.e., $M_y = -m_z = \frac{1}{2}$ for $n + {}^3$He and $M_y = -m_z = -\frac{1}{2}$ for $p + {}^3$H. Furthermore, ϵ_j, p_j, and $|\phi_j\rangle$ depend on M_y, implying that also the location of quasi-singularities of U_1 and the special integration weights [19] depend on M_y. Thus, the calculation of $|\phi_j\rangle$ and $U_1 G_0 t$ is done using the $|(T_x t_y)T_y M_y t_z m_z\rangle$ isospin basis. The two-nucleon transition matrix t is different for pp, np, and nn pairs. It preserves T_x but depends on its projection M_x, i.e., $\langle T'_x M'_x | t | T_X M_x \rangle = \delta_{T'_x T_x} \delta_{M'_x M_x} t_{T_x M_x}$. This gives rise to the coupling between $T_y = \frac{1}{2}$ and $\frac{3}{2}$ states, i.e., the nonvanishing components are

$$\langle (T_x t_y)T'_y M_y t_z m_z | t | (T_x t_y)T_y M_y t_z m_z \rangle$$
$$= \sum_{M_x} \langle T_x M_x t_y (M_y - M_x) | T'_y M_y \rangle$$
$$\times \langle T_x M_x t_y (M_y - M_x) | T_y M_y \rangle t_{T_x M_x}. \tag{7}$$

Abbreviating $\langle (T_x t_y)T'_y M_y t_z m_z | t | (T_x t_y)T_y M_y t_z m_z \rangle$ by $\langle T'_y | t(T_x, M_y) | T_y \rangle$, in terms of pp, np, and nn transition

operators t_{NN} we obtain

$$\langle T'_y | t(0, M_y) | T_y \rangle = \delta_{T'_y T_y} \delta_{T_y \frac{1}{2}} t_{np}, \tag{8a}$$

$$\left\langle \frac{1}{2} \left| t\left(1, \frac{1}{2}\right) \right| \frac{1}{2} \right\rangle = \frac{2}{3} t_{pp} + \frac{1}{3} t_{np}, \tag{8b}$$

$$\left\langle \frac{3}{2} \left| t\left(1, \frac{1}{2}\right) \right| \frac{1}{2} \right\rangle = \sqrt{\frac{2}{9}} (t_{pp} - t_{np}), \tag{8c}$$

$$\left\langle \frac{3}{2} \left| t\left(1, \frac{1}{2}\right) \right| \frac{3}{2} \right\rangle = \frac{1}{3} t_{pp} + \frac{2}{3} t_{np}, \tag{8d}$$

$$\left\langle \frac{1}{2} \left| t\left(1, -\frac{1}{2}\right) \right| \frac{1}{2} \right\rangle = \frac{2}{3} t_{nn} + \frac{1}{3} t_{np}, \tag{8e}$$

$$\left\langle \frac{3}{2} \left| t\left(1, -\frac{1}{2}\right) \right| \frac{1}{2} \right\rangle = \sqrt{\frac{2}{9}} (t_{np} - t_{nn}), \tag{8f}$$

$$\left\langle \frac{3}{2} \left| t\left(1, -\frac{1}{2}\right) \right| \frac{3}{2} \right\rangle = \frac{1}{3} t_{nn} + \frac{2}{3} t_{np}. \tag{8g}$$

In the $2 + 2$ configuration the two-nucleon transition matrix couples the states with different $\mathcal{T}$ but preserves the other isospin quantum numbers, i.e., the nonvanishing components are

$$\langle [T_x(t_y t_z)T_z]\mathcal{T}'\mathcal{M}_\mathcal{T} | t | [T_x(t_y t_z)T_z]\mathcal{T}\mathcal{M}_\mathcal{T} \rangle$$
$$= \sum_{M_x} \langle T_x M_x T_z (\mathcal{M}_\mathcal{T} - M_x) | \mathcal{T}'\mathcal{M}_\mathcal{T} \rangle$$
$$\times \langle T_x M_x T_z (\mathcal{M}_\mathcal{T} - M_x) | \mathcal{T}\mathcal{M}_\mathcal{T} \rangle t_{T_x M_x}. \tag{9}$$

The above operator, abbreviated by $\langle \mathcal{T}' | t(T_x, T_z, \mathcal{M}_\mathcal{T}) | \mathcal{T} \rangle$, can be expressed through t_{NN} as

$$\langle \mathcal{T}' | t(0, T_z, 0) | \mathcal{T} \rangle = \delta_{\mathcal{T}' T_z} \delta_{\mathcal{T} T_z} t_{np}, \tag{10a}$$

$$\langle 1 | t(1, 0, 0) | 1 \rangle = t_{np}, \tag{10b}$$

$$\langle 0 | t(1, 1, 0) | 0 \rangle = \frac{1}{3} (t_{pp} + t_{np} + t_{nn}), \tag{10c}$$

$$\langle 1 | t(1, 1, 0) | 0 \rangle = \frac{1}{\sqrt{6}} (t_{pp} - t_{nn}), \tag{10d}$$

$$\langle 1 | t(1, 1, 0) | 1 \rangle = \frac{1}{2} (t_{pp} + t_{nn}), \tag{10e}$$

$$\langle 2 | t(1, 1, 0) | 0 \rangle = \frac{1}{\sqrt{18}} (t_{pp} + t_{nn} - 2t_{np}), \tag{10f}$$

$$\langle 2 | t(1, 1, 0) | 1 \rangle = \frac{1}{\sqrt{12}} (t_{pp} - t_{nn}), \tag{10g}$$

$$\langle 2 | t(1, 1, 0) | 2 \rangle = \frac{1}{\sqrt{18}} (t_{pp} + 4t_{np} + t_{nn}). \tag{10h}$$

The nondiagonal isospin coupling in Eqs. (8) and (10) is due to the charge dependence of the underlying interaction, with the pp Coulomb repulsion yielding the dominant contribution. However, the $T_y = \frac{3}{2}$ and thereby also $\mathcal{T} = 2$ components resulting from this charge dependence in the $n + {}^3$He and $p + {}^3$H channel states are very small, of the order of 0.01%. The $d + d$ channel state is pure $\mathcal{T} = 0$ state. The $d + n + p$ breakup channel state is limited to $\mathcal{T} = 0$ and 1, and solely

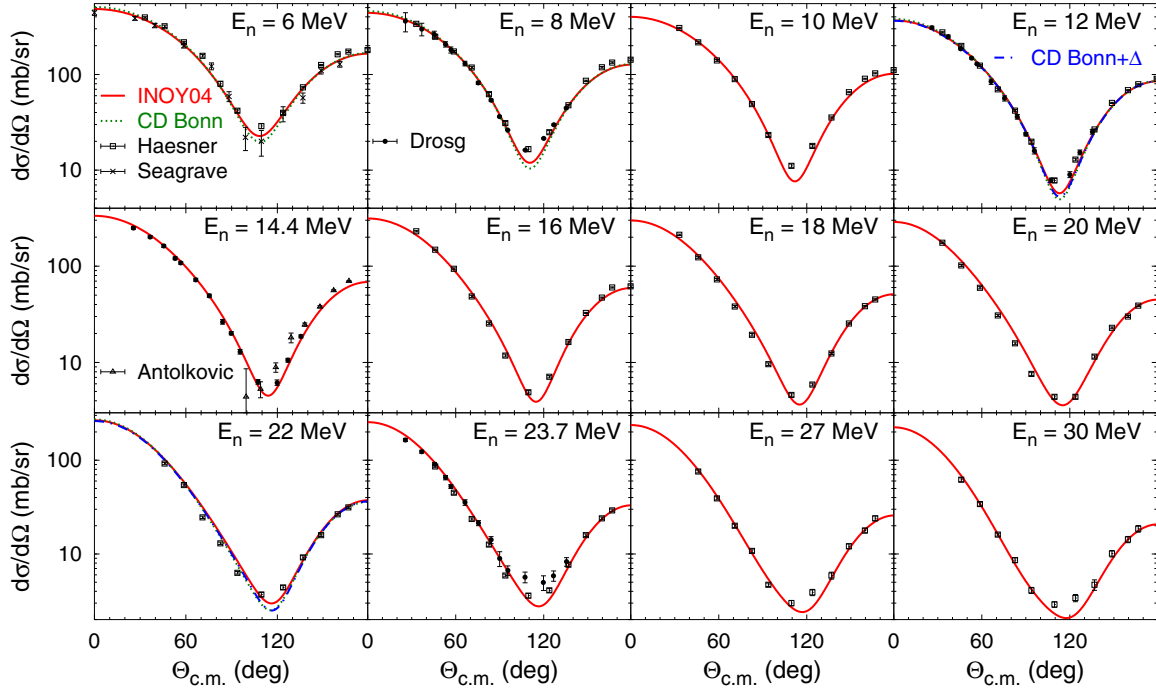FIG. 1. (Color online) Differential cross section of elastic n-^{3}He scattering at neutron energy between 6 and 30 MeV. Results obtained with potentials INOY04 (solid curves), CD Bonn (dotted curves), and CD Bonn $+ \Delta$ (dashed-dotted curves) are compared with data from Refs. [33–36].

the $n + n + p + p$ channel state may have moderate $\mathcal{T} = 2$ component. In fact, the leading contribution of $\mathcal{T} = 2$ states is of first order in the charge dependence for the four-cluster breakup amplitude but of second order, i.e., much smaller, for all other amplitudes. Thus, $\mathcal{T} = 2$ states can be safely neglected in the solution of the AGS equations if the four-cluster breakup amplitude is not explicitly calculated. This is in close analogy with $p + d$ scattering where the total isospin $\frac{3}{2}$ states can be safely neglected when calculating elastic scattering and total breakup cross section, but are important in particular kinematic configurations of breakup [29]. We therefore include only $\mathcal{T} = 0$ and 1 states in the present calculations of $n + {}^3$He scattering.

The results are well converged in terms of angular momentum states. At the highest considered neutron beam energy $E_n = 30$ MeV we include four-nucleon partial waves with $l_x, l_y \leqslant 5$, $l_z, j_x, j_y \leqslant 6$, $J_y \leqslant \frac{11}{2}$, and $\mathcal{J} = 7$. The most demanding observables are the $d + d$ transfer and breakup cross sections. The convergence for elastic and charge exchange reactions is faster. The number of partial waves can be reduced at lower energies and in lower $\mathcal{J}$ states.

III. RESULTS

We study the $n + {}^3$He scattering using several models of realistic high-precision NN potentials: the inside-nonlocal outside-Yukawa (INOY04) potential by Doleschall [5,30], the charge-dependent Bonn potential (CD Bonn) [31], and its coupled-channel extension CD Bonn $+ \Delta$ [32]. The latter allows for an excitation of a nucleon to a Δ isobar and thereby yields mutually consistent effective three- and four-nucleon

forces (3NF and 4NF). The ^{3}He (^{3}H) binding energy calculated with INOY04, CD Bonn, and CD Bonn $+ \Delta$ potentials is 7.73, 7.26, and 7.53 MeV (8.49, 8.00, and 8.28 MeV), respectively; the experimental value is 7.72 MeV (8.48 MeV). We therefore use INOY04 for predictions at all considered energies since this potential yields nearly the experimental value for the $3N$ binding energy. Other potentials are used at fewer selected energies to investigate the dependence of predictions on the force model. The calculations with the CD Bonn (CD Bonn $+ \Delta$) potential are performed only at neutron energies of 6, 8, 12, and 22 MeV (12 and 22 MeV).

In Fig. 1 we show the differential cross section $d\sigma/d\Omega$ for elastic $n + {}^3$He scattering as a function of the center of mass (c.m.) scattering angle $\Theta_{\text{c.m.}}$. The neutron energy E_n ranges from 6 to 30 MeV, the highest energy at which, to the best of our knowledge, exclusive data for elastic $n + {}^3$He scattering exist. The differential cross section decreases with the increasing energy and also changes the shape; the calculations describe the energy and angular dependence of the experimental data fairly well. There are disagreements between different data sets, in particular, between [33] and [34] at $E_n = 6$ MeV, between [35] and [36] at $E_n = 14.4$ MeV, and between [33] and [35] at $E_n = 23.7$ MeV. Only at $E_n = 14.4$ MeV it is quite obvious that the data [36] is inconsistent with other measurements and calculations.

It is interesting to compare the present $n + {}^3$He results with the ones for $p + {}^3$He elastic scattering [20], as there are several differences. First, the energy dependence is slower for $n + {}^3$He. Second, below 10 MeV the $n + {}^3$He data are well described at $\Theta_{\text{c.m.}} < 100°$ but slightly underpredicted at larger angles, while the $p + {}^3$He data are described well
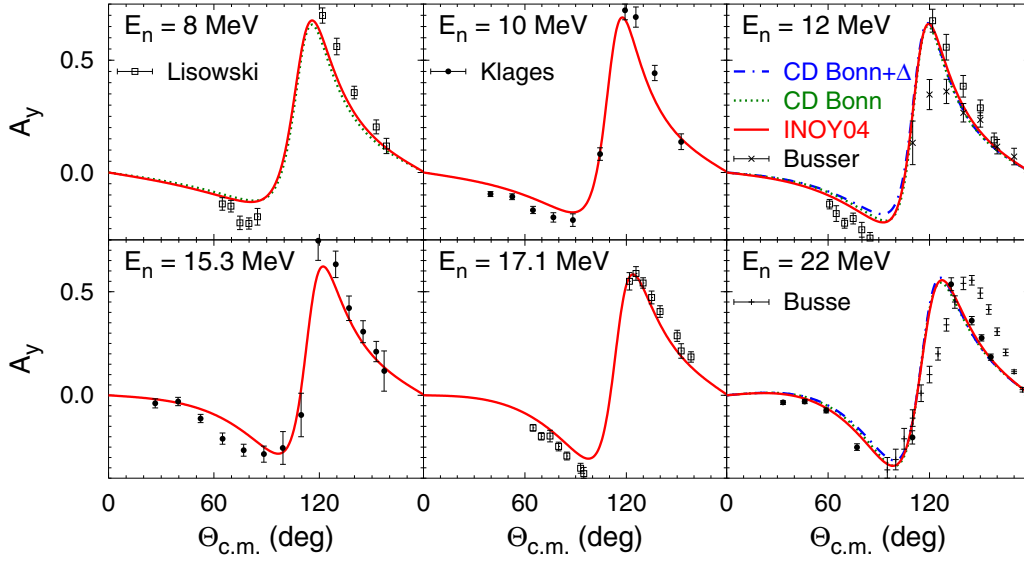
FIG. 2. (Color online) Neutron analyzing power of elastic n-³He scattering at neutron energy between 8 and 22 MeV. Curves as in Fig. 1. Data are from Refs. [40–43].

at $\Theta_{c.m.} > 60°$ with slight underprediction at smaller angles. On the other hand, both $n + $³He and $p + $³He data are well reproduced by the theory between 12 and 22 MeV in the whole angular regime, but the minimum of $d\sigma/d\Omega$ around $\Theta_{c.m.} = 120°$ gets underpredicted above 23 MeV. This may indicate a need to include an additional 3NF, as in the case of the nucleon-deuteron scattering [37,38]. The sensitivity to the potential model is similar in both $n + $³He and $p + $³He cases. It is insignificant beyond the minimum of $d\sigma/d\Omega$ that roughly scales with the ³He binding energy; a weaker binding corresponds to a deeper minimum. At $E_n = 12$ MeV the CD Bonn and CD Bonn $+ \Delta$ results are lower than those of INOY04 by 14% and 8%, respectively. At $E_n = 22$ MeV this correlation is violated, amounting to 18% reduction for both CD Bonn and CD Bonn $+ \Delta$ potentials. This may be due to an almost complete cancellation of two competing Δ-isobar contributions: the effective 3NF and the NN dispersion. While the former increases $d\sigma/d\Omega$ at the minimum by 15%, the latter decreases it by roughly the same amount. A partial cancellation between two-baryon dispersive and 3NF effects is a characteristic feature of the CD Bonn $+ \Delta$ model, seen also in previous studies [20,39].

In Fig. 2 we show the neutron analyzing power A_y for the elastic $n + $³He scattering at neutron energies ranging from 8 to 22 MeV. The qualitative reproduction of the experimental data by our calculations is reasonable, except for the data sets [42,43] that are incompatible also with other data [40,41]. Some discrepancies, decreasing as the energy increases, exist around the minimum and the maximum. The sensitivity to the nuclear force model and the energy dependence are quite weak. In all these respects, the behavior of the A_y in the elastic $n + $³He scattering is qualitatively the same as observed for the proton analyzing power in the $p + $³He elastic scattering [20].

To the best of our knowledge, there are no experimental data for other spin observables in the $n + $³He elastic scattering. Nevertheless, we calculated various spin correlation and spin transfer coefficients. In all studied cases we found only small

sensitivity of the predictions to the NN force model. As a characteristic example in Fig. 3 we present results for ³He target analyzing power A_{0y}, n-³He spin correlation coefficient A_{yy}, and neutron spin transfer coefficient K_y^y at $E_n = 12$ and 22 MeV. Comparing with the corresponding observables in the $p + $³He elastic scattering [20] we observe that some of them, such as A_{yy} and K_y^y, exhibit a very different angular dependence. This is not surprising given the fact that $n +$
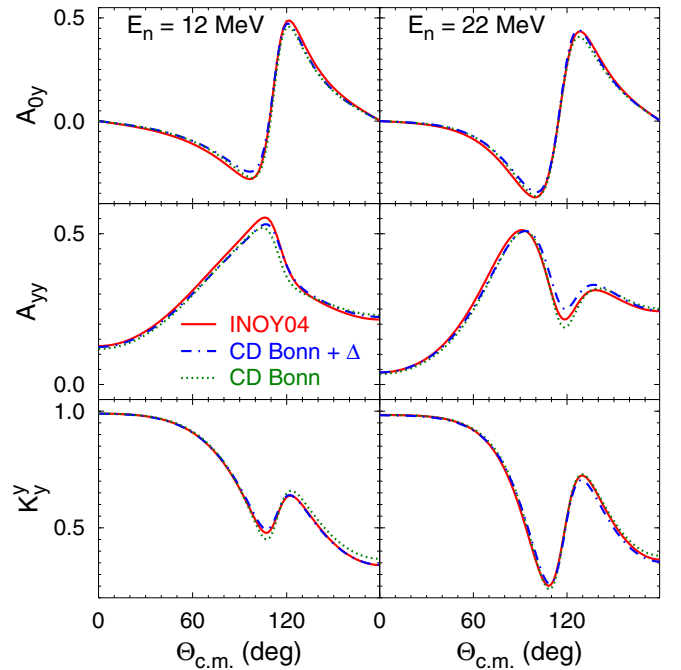

FIG. 3. (Color online) ³He target analyzing power A_{0y}, n-³He spin correlation coefficient A_{yy}, and neutron spin transfer coefficient K_y^y for elastic $n + $³He scattering at 12 and 22 MeV neutron energy. Curves as in Fig. 1.

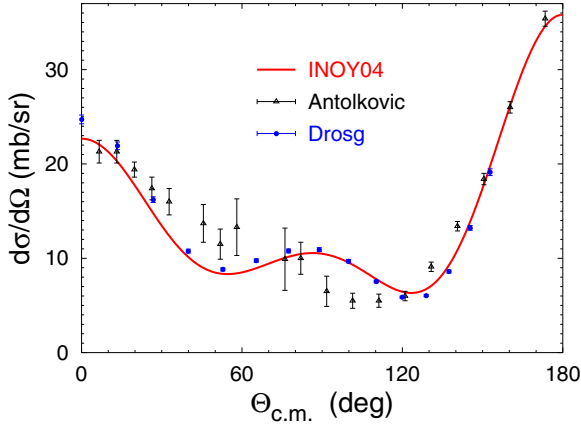FIG. 4. (Color online) Differential cross section of the $^3\mathrm{He}(n,p)^3\mathrm{H}$ reaction at 14.4 MeV neutron energy. Predictions using INOY04 potential are compared with the data from Refs. [36,44].

FIG. 5. (Color online) Differential cross section of the $^3\mathrm{He}(n,d)^2\mathrm{H}$ reaction at $E_n = 14.4$ MeV. Predictions using INOY04 potential are compared with the data from Ref. [36].

$^3\mathrm{He}$ scattering involves both total isospin $\mathcal{T} = 0$ and 1 states while $p + {}^3\mathrm{He}$ is restricted to $\mathcal{T} = 1$. On the other hand, this indicates that accurate measurements of n-$^3\mathrm{He}$ spin correlation and/or spin transfer coefficients that differ significantly from previously studied observables may test the nuclear interaction in a novel way.

Next we consider rearrangement reactions initiated by $n + {}^3\mathrm{He}$ collisions. We present here only two examples for $^3\mathrm{He}(n,p)^3\mathrm{H}$ and $^3\mathrm{He}(n,d)^2\mathrm{H}$ processes measured at $E_n = 14.4$ MeV in Ref. [36], since most experiments are performed for the time reversed reactions $^3\mathrm{H}(p,n)^3\mathrm{He}$ and $^2\mathrm{H}(d,n)^3\mathrm{He}$ that will be studied elsewhere. In Fig. 4 we show the differential cross section $d\sigma/d\Omega$ for the charge exchange reaction $^3\mathrm{He}(n,p)^3\mathrm{H}$ at $E_n = 14.4$ MeV. The theoretical predictions agree with the data [36] only at forward and backward angles. On the other hand, the data [44] transformed from the time reversed reaction $^3\mathrm{H}(p,n)^3\mathrm{He}$ at $E_n = 14.0$ MeV is in a considerably better agreement with our predictions. In particular, the shape of the observable with two local minima is well described by the theory, as found in our preliminary calculations for the $^3\mathrm{H}(p,n)^3\mathrm{He}$ reaction [45]. Thus, very likely the data points from Ref. [36] at intermediate angles are inaccurate.

In Fig. 5 we show the differential cross section $d\sigma/d\Omega$ for the transfer reaction $^3\mathrm{He}(n,d)^2\mathrm{H}$ at $E_n = 14.4$ MeV. The observable is symmetric with respect to $\Theta_{\mathrm{c.m.}} = 90°$ and peaks at forward and backward directions. The overall agreement between theoretical calculations and the data [36] is fair, given the large error bars and, possibly, further inaccuracies in the data [36], especially at intermediate angles where $d\sigma/d\Omega$ is small and has several local extrema. To draw a more definite conclusion on transfer reactions, calculations and analysis of $^2\mathrm{H}(d,n)^3\mathrm{He}$ and $^2\mathrm{H}(d,p)^3\mathrm{H}$ reactions need to be accomplished.

Finally, in Fig. 6 we show the energy dependence of the $n + {}^3\mathrm{He}$ total and partial cross sections σ_x for all open channels, i.e., elastic, charge exchange, transfer, and breakup. This extends our previous results [45] up to $E_n = 30$ MeV. The theoretical predictions are below the data in the regime
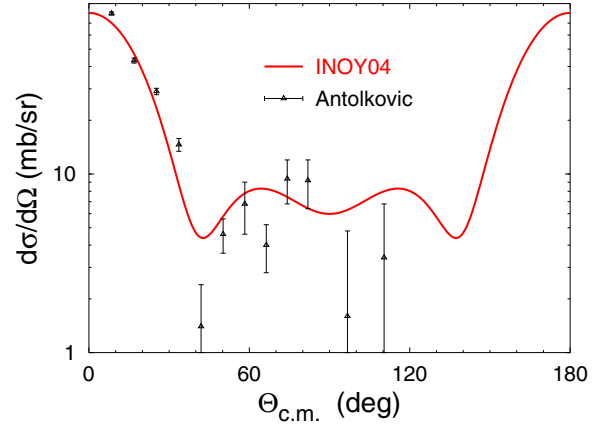
$E_n < 5$ MeV where several resonant $4N$ states exist and whose location is not well predicted by the underlying force models as discussed in Refs. [12,49]. On the contrary, the agreement is nearly perfect at higher energies up to 22 MeV, but moderate discrepancies arise in $^3\mathrm{He}(n,p)^3\mathrm{H}$ and $^3\mathrm{He}(n,d)^2\mathrm{H}$ cross sections above $E_n = 25$ MeV. The total breakup cross section, including both three- and four-cluster channels, increases rapidly with energy, and above $E_n = 23$ MeV exceeds σ_x for all other inelastic channels. The experimental data for the total breakup cross section [35] are in agreement with theoretical predictions, although the data point at $E_n = 7.9$ MeV is inconclusive owing to very large error bars.

IV. SUMMARY

We considered neutron-$^3\mathrm{He}$ scattering at neutron energies ranging from 6 to 30 MeV. We solved the Alt, Grassberger, and Sandhas equations for the symmetrized four-nucleon transition operators in the momentum-space framework. We included the
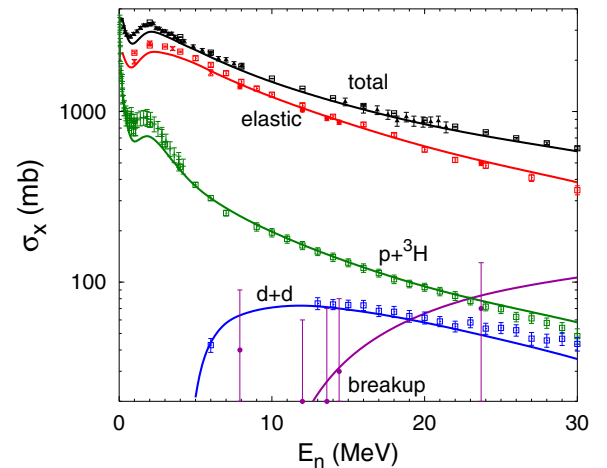

FIG. 6. (Color online) n-$^3\mathrm{He}$ total and partial cross sections as functions of the neutron beam energy calculated using the INOY04 potential. The data are from Refs. [33,46] (□), [34] (×), [35] (●), [47] (▲), and [48] (+).

pp Coulomb force and used several realistic *NN* potentials. The complicated singularities in the kernel of AGS equations above breakup threshold were treated by the complex energy method with special integration weights. Fully converged results were obtained not only for elastic $n + {}^3$He scattering, but also for inelastic reactions. Furthermore, total cross sections for all reaction channels were calculated, showing the importance of breakup at higher energies.

The overall agreement between the theoretical predictions and the experimental data is good. Few moderate discrepancies exist in the extrema of elastic analyzing power and differential cross section, similar to the case of elastic proton-^{3}He scattering. The charge exchange and transfer reactions will be analyzed in more detail through time-reverse processes ^{3}H(p,n)^{3}He and ^{2}H(d,n)^{3}He; the respective calculations are in progress.

[1] D. R. Tilley, H. Weller, and G. M. Hale, Nucl. Phys. A **541**, 1 (1992).

[2] M. Viviani, A. Kievsky, S. Rosati, E. A. George, and L. D. Knutson, Phys. Rev. Lett. **86**, 3739 (2001).

[3] A. Kievsky, S. Rosati, M. Viviani, L. E. Marcucci, and L. Girlanda, J. Phys. G **35**, 063101 (2008).

[4] O. A. Yakubovsky, Yad. Fiz. **5**, 1312 (1967) [Sov. J. Nucl. Phys. **5**, 937 (1967)].

[5] R. Lazauskas and J. Carbonell, Phys. Rev. C **70**, 044002 (2004).

[6] P. Grassberger and W. Sandhas, Nucl. Phys. B **2**, 181 (1967); E. O. Alt, P. Grassberger, and W. Sandhas, JINR Report No. E4-6688, 1972 (unpublished).

[7] A. Deltuva and A. C. Fonseca, Phys. Rev. C **75**, 014005 (2007).

[8] A. Deltuva and A. C. Fonseca, Phys. Rev. Lett. **98**, 162502 (2007).

[9] M. Viviani, A. Deltuva, R. Lazauskas, J. Carbonell, A. C. Fonseca, A. Kievsky, L. E. Marcucci, and S. Rosati, Phys. Rev. C **84**, 054010 (2011).

[10] R. Lazauskas, Phys. Rev. C **79**, 054007 (2009).

[11] M. Viviani, R. Schiavilla, L. Girlanda, A. Kievsky, and L. E. Marcucci, Phys. Rev. C **82**, 044001 (2010).

[12] A. Deltuva and A. C. Fonseca, Phys. Rev. C **76**, 021001(R) (2007).

[13] A. Deltuva and A. C. Fonseca, Phys. Rev. C **81**, 054002 (2010).

[14] R. Lazauskas and J. Carbonell, Phys. Rev. C **84**, 034002 (2011).

[15] R. Lazauskas, Phys. Rev. C **86**, 044002 (2012).

[16] V. D. Efros, W. Leidemann, and G. Orlandini, Phys. Lett. B **338**, 130 (1994).

[17] H. Kamada, Y. Koike, and W. Glöckle, Prog. Theor. Phys. **109**, 869 (2003).

[18] R. Lazauskas (private communication).

[19] A. Deltuva and A. C. Fonseca, Phys. Rev. C **86**, 011001(R) (2012).

[20] A. Deltuva and A. C. Fonseca, Phys. Rev. C **87**, 054002 (2013).

[21] E. Uzu, H. Kamada, and Y. Koike, Phys. Rev. C **68**, 061001(R) (2003).

[22] J. R. Taylor, Nuovo Cimento B **23**, 313 (1974); M. D. Semon and J. R. Taylor, Nuovo Cimento A **26**, 48 (1975).

[23] E. O. Alt and W. Sandhas, Phys. Rev. C **21**, 1733 (1980).

[24] A. Deltuva, A. C. Fonseca, and P. U. Sauer, Phys. Rev. C **71**, 054005 (2005).

[25] L. Schlessinger, Phys. Rev. **167**, 1411 (1968).

[26] K. Chmielewski, A. Deltuva, A. C. Fonseca, S. Nemoto, and P. U. Sauer, Phys. Rev. C **67**, 014002 (2003).

[27] A. Deltuva, Phys. Rev. A **85**, 012708 (2012).

[28] A. Deltuva and A. C. Fonseca, Phys. Rev. C **87**, 014002 (2013).

[29] A. Deltuva, A. C. Fonseca, and P. U. Sauer, Phys. Rev. C **72**, 054004 (2005).

[30] P. Doleschall, Phys. Rev. C **69**, 054001 (2004).

[31] R. Machleidt, Phys. Rev. C **63**, 024001 (2001).

[32] A. Deltuva, R. Machleidt, and P. U. Sauer, Phys. Rev. C **68**, 024005 (2003).

[33] B. Haesner, W. Heeringa, H. O. Klages, H. Dobiasch, G. Schmalz, P. Schwarz, J. Wilczynski, B. Zeitnitz, and F. Käppeler, in *EXFOR Database* (NNDC, Brookhaven, 1982).

[34] J. D. Seagrave, L. Cranberg, and J. E. Simmons, Phys. Rev. **119**, 1981 (1960).

[35] M. Drosg, D. K. McDaniels, J. C. Hopkins, J. D. Seagrave, R. H. Sherman, and E. C. Kerr, Phys. Rev. C **9**, 179 (1974).

[36] B. Antolkovic, G. Paic, P. Tomaš, and D. Rendic, Phys. Rev. **159**, 777 (1967).

[37] H. Witała, W. Glöckle, D. Hüber, J. Golak, and H. Kamada, Phys. Rev. Lett. **81**, 1183 (1998).

[38] S. Nemoto, K. Chmielewski, S. Oryu, and P. U. Sauer, Phys. Rev. C **58**, 2599 (1998).

[39] A. Deltuva, A. C. Fonseca, and P. U. Sauer, Phys. Lett. B **660**, 471 (2008).

[40] P. Lisowski, T. Rhea, R. Walter, C. Busch, and T. Clegg, Nucl. Phys. A **259**, 61 (1976).

[41] H. O. Klages, W. Heeringa, H. Dobiasch, B. Fischer, B. Haesner, P. Schwarz, J. Wilczynski, and B. Zeitnitz, Nucl. Phys. A **443**, 237 (1985).

[42] F. Büsser, H. Dubenkropp, F. Niebergall, and K. Sinram, Nucl. Phys. A **129**, 666 (1969).

[43] W. Busse, B. Efken, D. Hilscher, H. Morgenstern, and J. Scheer, Nucl. Phys. A **187**, 21 (1972).

[44] M. Drosg, Nucl. Sci. Eng. **67**, 190 (1978); in *EXFOR Database* (NNDC, Brookhaven, 1978).

[45] A. Deltuva and A. C. Fonseca, Phys. Rev. Lett. **113**, 102502 (2014).

[46] B. Haesner, W. Heeringa, H. O. Klages, H. Dobiasch, G. Schmalz, P. Schwarz, J. Wilczynski, B. Zeitnitz, and F. Käppeler, Phys. Rev. C **28**, 995 (1983).

[47] M. E. Battat *et al.*, Nucl. Phys. **12**, 291 (1959).

[48] J. H. Gibbons and R. L. Macklin, Phys. Rev. **114**, 571 (1959).

[49] A. C. Fonseca, G. Hale, and J. Haidenbauer, Few-Body Syst. **31**, 139 (2002).